УДК 539.1.05 + 539.1.074.22

THE FORWARD DETECTOR OF THE ANKE SPECTROMETER. TRACKING SYSTEM AND ITS USE IN DATA ANALYSIS

S. Dymov [a], *W. Erven* [b], *A. Kacharava* [a,c], *R. Koch* [d], *V. Komarov* [a], *A. Kulikov* [a], *V. Kurbatov* [a], *G. Macharashvili* [a], *H. Ohm* [d], *A. Petrus* [a], *F. Rathmann* [d], *H. Seyfarth* [d], *H. Ströher* [d], *S. Yaschenko* [a,c], *B. Zalikhanov* [a], *K. Zwoll* [b]

[a] Joint Institute for Nuclear Research, Dubna

[b] Zentrallabor für Elektronik, Forschungszentrum Jülich, Germany

[c] Physikalisches Institut II, Universität Erlangen-Nürnberg, Germany

[d] Institut für Kernphysik, Forschungszentrum Jülich, Germany

The tracking system of the forward detector of the ANKE magnetic spectrometer at the internal beam of the accelerator COSY (Jülich, Germany) is described. Data analysis procedures, including track search and momentum reconstruction, are presented, and the performance of the tracking system is illustrated with the use of experimental data.

Описывается трековая система переднего детектора магнитного спектрометра ANKE, расположенного на внутреннем пучке ускорителя COSY (Юлих, Германия). Представлены применяемые процедуры обработки данных, включая поиск треков и восстановление импульса. Характеристики трековой системы проиллюстрированы с использованием экспериментальных данных.

INTRODUCTION

A brief description of the forward detector (FD) system of the ANKE spectrometer [1] has been given in [2]. The main content of Ref. [2] was design and performance of the counter hodoscopes of the FD. Here we describe the FD tracking system: fast multiwire proportional chambers (MWPC) and the relevant software for track reconstruction. The achieved performance in momentum reconstruction and identification of single- and double-particle events is presented as well.

1. THE TRACKING SYSTEM

1.1. Main Hardware Components. Figure 1 presents the part of the ANKE setup intended for detection of charged particles in the FD and reconstruction of their trajectories and momenta. Particles produced in the beam–target interaction pass through the vacuum chamber of the spectrometric magnet D2, leaving it through the forward exit window. They are detected in a set of three multiwire proportional chambers (MWPC) and a scintillation counter hodoscope [2]. In addition to the hits on the MWPC sensitive planes, the positions of the hit hodoscope counters and the time difference between signals from the photomultipliers (PMs) viewing the scintillators from the top and the bottom are used in the track reconstruction procedure. MWPCs, the key component of the tracking system, are described in more detail below.

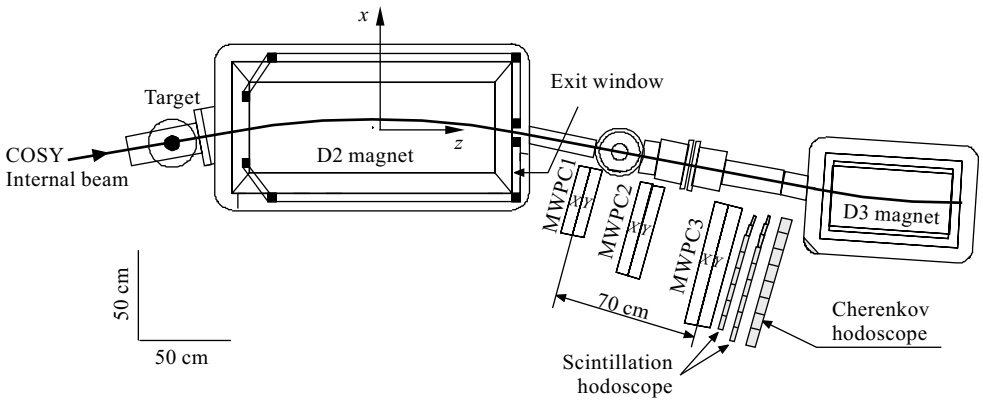

Fig. 1. Top view of the forward detector at ANKE

1.2. Description of the MWPCs. The forward detector is located between the spectrometric dipole D2 and the exit dipole D3 of the ANKE magnetic system (Fig. 1). The available space is rather limited there: the gap between the dipoles is 1.6 m in length, and the distance between the accelerator beam tube and the ANKE side detector is about 0.7 m. Such a position results in severe requirements for the tracking system. Due to closeness to the beam pipe, it must be able to operate at rather high counting rates ($> 10^5$ s^{-1}). In addition, because of a short distance between the MWPCs, one has to achieve a sufficiently high spatial resolution (better than 1 mm). Detection of particles emitted at small angles and high momenta is required in a number of experiments at ANKE. These particles pass the detector region close to the beam pipe, which means that the chamber frame width must be minimized on the beam pipe side.

To satisfy these requirements, we have developed multiwire proportional chambers [3, 4] with a small anode–cathode gap, filled with a fast gas mixture of CF_4 + iso-C_4H_{10} and containing a supporting foil for anode wires. To provide the needed spatial resolution, a signal wire step of 1 mm was chosen which is usually difficult to combine with a rather large chamber size (about 60 cm). Electromagnetic stability of the chambers [5] is achieved by the use of a high-resistance foil supporting the wires. The chamber assembling technology is described in [6].

The FD system comprises three MWPCs in total. Each of them is a package containing one X and one Y module. Every module contains a wire and a strip plane. In what follows, the planes located in an $X(Y)$ module will be referred to as the $X(Y)$. Wires are oriented vertically in the X wire planes, and horizontally in the Y planes. The strips are inclined by 18° with respect to the vertical axis in the X planes, and by -18° in the Y planes. The MWPCs are mounted on a common support frame with the hodoscope.

The layout of the chamber module is shown in Fig. 2, the design parameters are given in table.

The drift electrode (*1*) (Fig. 2) is made of a carbon-coated mylar foil, which is fastened to the rods (*2*). Negative voltage $U_1 = 2.8$ kV at the electrode provides field for the electrons drift towards the anode wires which are held at the zero potential. The cathode plane (*4*)

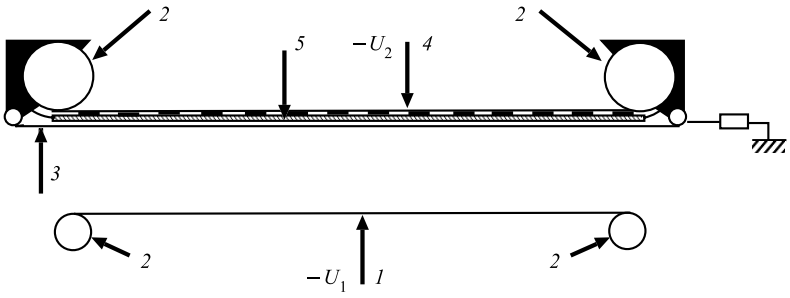

Fig. 2. Schematic layout of an MWPC module: *1* — drift electrode; *2* — holding rods; *3* — anode wires; *4* — mylar cathode foil with strips; *5* — high-resistance foil

consists of a mylar foil covered with conductive silver paint strips. The strips are held at a negative potential $U_2 = 1.7$ kV, and are separated from the anode wires (*3*) by a high-resistance foil (*5*) made of varnished cloth. Conductivity of the foil was achieved initially by diffusion of iodine from an iodine alcoholic solution. To keep the foil resistance in the needed range, an isopropyl alcohol was later added to the gas mixture. The resulting mixture is $80\,\%\mathrm{CF_4} + 17\,\%\mathrm{C_4H_{10}} + 3\,\%\mathrm{C_3H_8O}$.

Parameters of the MWPCs

	MWPC1	MWPC2	MWPC3
Sensitive area, cm	33×26	44×34	53×41
Anode wires	$\varnothing$ 20 μ, gold plated W+Re		
Anode wire step, mm	1.05		
Strip step, mm	3.15		
Drift electrode to wire plane distance, mm	1.5	2.0	2.5
Resistance of the high-resistance foil, $\Omega \cdot \mathrm{cm}$	10^9		
Thickness in radiation length units	$0.46\,\%$ each MWPC		

The chamber operation differs significantly from that of conventional proportional chambers, as described in [7]. The chambers produce signals 6 ns long (FWHM) for the wire planes and 30 ns long for the strip ones. The time jitter of the signals is small, being around 8 ns for the wire pulses. This allows effective operation with short strobe signals. At the setup, the time resolution of the tracking system is limited by the readout electronics [8] which needs strobes more than 50 ns wide (while the chambers themselves could work with much shorter strobe pulses). The average number of wires fired by a crossing particle (cluster width) is close to one, which leads to high precision for coordinate measurements.

1.3. Main Software Components. The software for the analysis of FD data includes a code for finding tracks and reconstructing particle momenta, programs for calibration of the energy

losses in the hodoscope and the momentum-dependent Cherenkov counter registration efficiency (the operation of the counters is described in Ref. [2]), and a GEANT-based simulation program [9]. An important requirement for the tracking system is that the track coordinates must be known in the ANKE coordinate system with a rather high (~ 1 mm) precision. As a result, a special off-line procedure of geometrical alignment is used for calibration of the momentum scale. Additionally, a rather low and inhomogeneous efficiency of the MWPCs ($80{-}90\,\%$ in average) requires a sophisticated procedure for efficiency determination.

In Sec. 2 we describe the algorithms used for track and momentum reconstruction, and discuss details on momentum calibration and MWPC efficiency determination.

2. DATA ANALYSIS PROCEDURES

2.1. Track Search Conditions. The coordinate system is fixed to the D2 dipole, with the origin in its vacuum chamber center and the axes parallel to the dipole sides: the Z-axis is directed along the beam, the Y-axis is directed upwards, and the X-axis forms a right-hand coordinate system (see Fig. 1).

The average width of clusters in the MWPC wire planes is around 1.1 wire (≈ 1.1 mm). These planes measure three horizontal and three vertical track coordinates. The strip planes produce clusters of about three strips on average (≈ 1 cm cluster width), and measure six inclined track coordinates. Each plane of the hodoscope provides additional input for the track search: an X-coordinate with an accuracy of a counter width (4–8 cm), and a Y-coordinate with an accuracy (RMS) of 2–3 cm. The latter is obtained from the analysis of the arrival time of signals from the upper and lower photomultipliers of the counters.

The particle trajectory between the first MWPC and the hodoscope is very close to the straight line. Deviations caused by the fringe magnetic field are estimated to be only 0.6 mm for particles with a momentum of 0.4 GeV/c (the lowest momentum in the FD acceptance under the measurement conditions of ANKE experiments). The multiple scattering of the particles occurring between the MWPCs can be neglected during the track search (while the scattering in the 0.5-mm-thick aluminum exit window of D2 affects considerably the reconstructed momentum resolution). A straight-line model for the track is used in this region, and the line is described by four parameters $\mathbf{T} = (\tan\theta_{xz}, \tan\theta_{yz}, x_w, y_w)$. Here x_w, y_w are the X- and Y-coordinates of the track at the exit window surface (this surface is flat and perpendicular to the Z-axis); θ_{xz}, θ_{yz} are the projection angles onto the relevant planes.

With the simplest triggering for at least one particle detected in the FD, only one track is recorded in MWPCs in more than $99\,\%$ of events. At the same time, the average number of wire clusters on a plane is 1.7 per event. These figures reflect the situation of the normal background condition and a normal level of noise from the MWPC readout electronics.

2.2. The Track Finding Algorithm. To achieve the required three-momentum reconstruction accuracy, one has to draw the straight track through the wire clusters; thus, a track has to contain at least two clusters in the X wire planes, and two clusters in the Y wire planes. On the other hand, because of substantial inefficiency of the MWPCs, one should not request the presence of clusters from all wire and strip planes for a track. As a result, a track is sought on the MWPCs as a combination of clusters from two X and two Y wire planes as a minimum, and from all the wire and strip planes in the best case. Because of a

soft requirement for the minimum track contents, several concurrent track candidates can be constructed, and we use the following criteria to select the best one: the maximum number of wire clusters from different planes used to build the track (N_w), the best confidence level of the straight-line fit (CL), and the maximum value $\overline{E} = \prod(1 - \varepsilon_i)$, where ε_i is the efficiency of a plane at the point where it is crossed by the track. The product is calculated over all the wire and strip planes where no cluster is included into the track (the planes that are supposed to be inefficient). A comparison of $\overline{E}$ values of different tracks would be equivalent to a comparison of the number of inefficient wire and strip planes for these tracks in the case of equal and homogeneous MWPC efficiency.

The track is built by the following procedure: at the beginning we use only the information from the wire planes and the hodoscope to draw a space straight line, and then employ the information from the planes of inclined strips. The horizontal projection including clusters on two X wire planes and counters fired is drawn first, and clusters on two Y wire planes are then included to define the vertical projection.

Let us consider the track search algorithm in more detail. As the first step, we include into the track the responding counters, and use them together with the MWPC1 sensitive area boundaries to build a wide horizontal corridor for cluster search on the MWPCs. Then, a cluster is chosen from one of the X wire planes within this corridor, and the corridor is narrowed. A wire cluster from another X wire plane is chosen within the new corridor and is included into the track. A straight line in the XZ plane drawn through these two clusters must cross the counters selected and the sensitive area of all MWPCs. Similarly, two clusters from two Y wire planes are chosen, and the resulting space straight line is checked for crossing the counters and MWPCs. This line, together with its parameter errors, is used to determine a narrow (5–10 mm wide) search corridor on the strip and the rest of the wire planes. Once all the MWPC sensitive planes have been considered, we fit the collection of wire and strip clusters by the straight line, and calculate the $\overline{E}$ value of the track. Soft cuts are imposed on CL and $\overline{E}$, each of them rejecting estimated $0.5\,\%$ of tracks.

The first track candidate that includes the information (i. e., clusters or their absence) from all the planes and passes the cuts is kept as «the best». The following candidates are compared with it by a combination of N_w, CL and $\overline{E}$ values. A candidate can replace «the best» one in any of the following three cases (the index c refers to the track candidate considered, and the index b is for «the best» one):

1. $\overline{E}_c > \overline{E}_b - K_{\overline{E}}$ and $N_c^w > N_b^w$, where $K_{\overline{E}}$ is a constant;
2. $N_c^w = N_b^w$ and $\overline{E}_c > \overline{E}_b + K_{\overline{E}}$;
3. $N_c^w = N_b^w$, $\overline{E}_c > \overline{E}_b - K_{\overline{E}}$ and $\mathrm{CL}_c > \mathrm{CL}_b$.

The value of $K_{\overline{E}}$ is determined experimentally during the algorithm outcome optimization.

The schematic flow chart for track building is shown in Fig. 3. The above-described sequence of inclusion of the wire planes is realized in the block «Take the next plane». The tests done at different track construction steps are reflected by the block «Is the track OK?», and the criteria of «the best» candidate replacement are included into the «Can replace the best track?» block. The block «Exclude ..., return to the previous plane» restores the cluster search corridors determined before processing the information from the last included plane.

The candidate that appears to be «the best» after consideration of all combinations is accepted as the track found. After that, the clusters on the wire planes used to build this

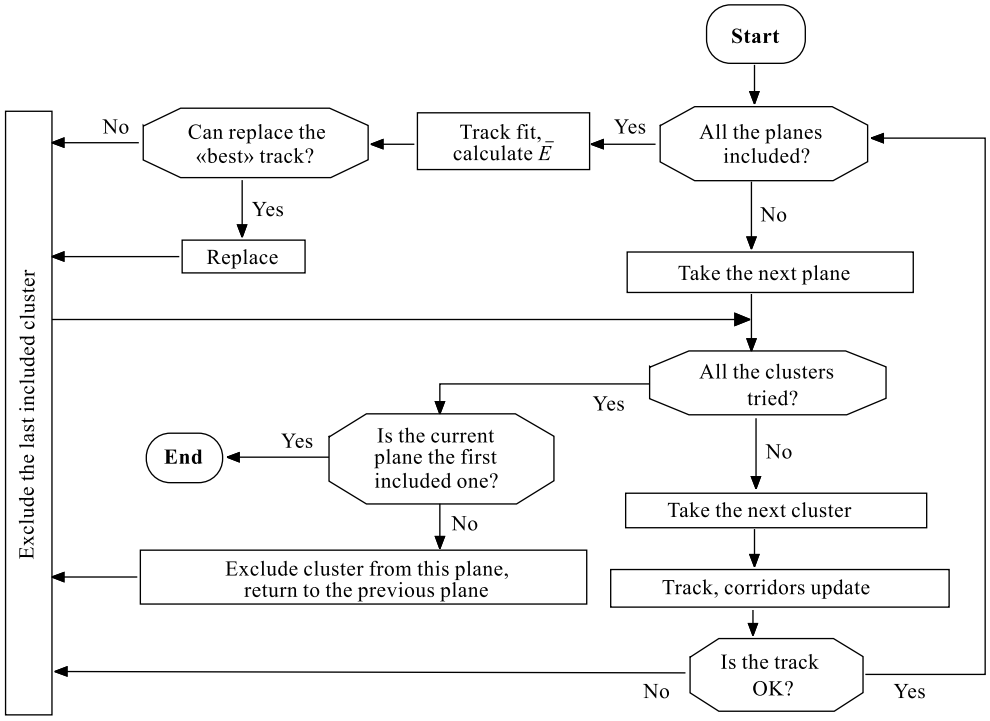

Fig. 3. Track building scheme

candidate, are excluded from the search, and the procedure starts again. Exclusion of the clusters is admissible because the wire step and the wire cluster size are small, so that the probability of losing tracks which are closely located on MWPC planes is low enough.

2.3. Momentum Reconstruction. The magnetic field of D2 has been measured on a three-dimensional grid, allowing one to reconstruct the ejectile 3-momenta at the production point. A number of reconstruction methods are adopted for the ANKE forward detector, including the box-field approximation, tracing with the Runge–Kutta method, use of neural networks, and a «polynomial» approximation. The latter method is chosen for the data analysis due to a high calculation speed and a sufficient quality of the approximation. The method consists in expression of the components of the 3-momentum in the form of a polynomial of the measured parameters; we use its modification similar to the one described in Ref. [10].

Each of the momentum components is approximated by a third-order polynomial of the four track parameters $\mathbf{T}$. The polynomial coefficients are found from the teaching sample of events, produced by the GEANT-based simulation program. The sample is generated for every combination of the magnetic field value, the beam and the target positions used in the experiments.

The accuracy of the reconstruction method was studied for a set of simulated events obtained without introduction of experimental smearing factors (multiple scattering, MWPC coordinate resolution, size of the beam–target overlap). For such events the accuracy (RMS) of the reconstructed momentum was 5 to 10 times better than that for a set obtained with

full smearing (the experimental momentum resolution is described in Subsec. 3.3 and shown in Fig. 9). At the same time the maximum deviation of the average of the reconstructed momentum was less than $0.1\,\%$.

2.4. Momentum Scale Calibration. The trajectory bending angle in the magnetic field for the particles detected in the FD is rather small ($\approx 20^\circ$). This, together with a rather short distance between the chambers, leads to a high sensitivity of the reconstructed momentum value to the measured coordinates. The positions of the MWPCs in the ANKE coordinate system are measured mechanically with a 2 mm precision, whereas, for instance, for a 2 GeV/c particle an error of 2 mm in the position of MWPC1 (in the X-direction) leads to about 100 MeV/c change in the reconstructed momentum. At the same time, the required precision (accuracy of the average) of the momentum is normally better than 10 MeV/c. To achieve this, we apply a procedure of setup geometrical parameter tuning.

As the parameters to be adjusted, the X-coordinates of a pair of MWPCs have been chosen, since the reconstructed momentum value is most sensitive to them. We consider these coordinates as effective parameters, assuming that all other inaccuracies are corrected by an appropriate choice of these parameters. It is enough to align the positions of a pair of MWPCs, the position of the third chamber can then be found by using straight tracks.

To calibrate the momentum scale, we select several processes with completely reconstructable kinematics, and fit the effective parameters to obtain the correct missing mass values in these reactions. The choice of the reactions depends on the measurement conditions. Among the processes with one particle detected in the FD, the $pp \to pp$ and $pp \to d\pi^+$ reactions are used. One can also use several reactions with two particles detected, such as $pp \to d\pi^+$, $pp \to pp\pi^0$ and $pp \to pn\pi^+$ with an H_2 target, and $pd \to dn\pi^+$, $pd \to ppn$ and $pd \to {}^3\mathrm{H}\pi^+$ with a D_2 target. Examples of identification of the processes mentioned are brought in Subsecs. 3.2 and 3.4.

For illustration, let us consider application of this procedure to a data set obtained with an H_2 target at beam energies of 0.5 and 2.65 GeV. Events from the $pp \to pp$, $pp \to d\pi^+$ processes at both energies and $pp \to pn\pi^+$ at $T_p = 2.65$ GeV were used, and both charged ejectiles were detected in the reactions $pp \to d\pi^+$ and $pp \to pn\pi^+$ at $T_p = 2.65$ GeV. In this case the accuracies achieved after the tuning of the parameters were comprehensively studied. The study showed that the residual systematic shift of the mean momentum value $\Delta\langle p\rangle$ was less than a half of the momentum resolution $\sigma(p)$. For protons $\Delta\langle p\rangle/p < 0.5\,\%$, too. At the same time the residual deviations of the reconstructed missing mass values did not exceed 11 MeV.

2.5. Correction for MWPC Inefficiency. The average efficiency of a sensitive plane is $80{-}90\,\%$. This is caused by a short duration of the signal from the wire planes, which is not optimal for the readout electronics used. Under these conditions, the properties of the high-resistance foil lead to an inhomogeneous effficiency distribution over the plane surface. To account for such an inhomogeneity, one has to determine the efficiency map for each sensitive plane. The correction factor can then be calculated for each event by using the ε value for the plane region crossed by the track.

For obtaining the efficiency map of a sensitive plane, the sensitive area is divided into 20×20 rectangular cells (2–3 cm in size), and the efficiency is calculated for each cell. To do that, we build tracks using the other two MWPCs, and the probability to find a hit is calculated for each track crossing this cell. Only events with a single cluster on each of the wire planes are used to build the tracks.

This procedure requires a large amount of experimental data to achieve reasonable statistics in each cell on each plane. The statistical error of the efficiency value is below $1\,\%$ for the central part of the chambers and about $10\,\%$ for the edge cells in the case of 10 million events used. The sources of systematic errors are (i) presence of noise clusters on the plane where ε is estimated, (ii) false tracks used for the hit search, (iii) significant change in ε within a single cell, (iv) dependence of the detection efficiency on the energy loss. A detailed investigation has shown that in the first two cases the errors do not exceed 2–3 %. The third factor, if found important, can be suppressed by exclusion of the most inhomogeneous parts of the MWPC planes from the data analysis. The last factor can be controlled by selecting the type and momentum of the particles used for determination of ε.

3. PROCESSING OF EXPERIMENTAL DATA

3.1. Background Rejection Criteria. To reject the background, some obvious cuts, common for all experiments, are applied to the tracks reconstructed in the FD. They include (i) a cut on the Y track coordinates on the hodoscope planes, (ii) a requirement of crossing the D2 exit window, and (iii) a correct correlation of the track parameters in the YZ plane (the «vertical cut»). In the first case the coordinate of the line drawn using MWPCs information is compared to the coordinate calculated from the time difference between the upper and lower PMs of a counter. If two particles hit the same counter, the timing information may be distorted. For this reason this cut is not used during the track search but is applied when one makes sure that the counter is hit by a single particle. The «vertical cut» condition arises from smallness of the field components B_x and B_z, so the projection of the whole trajectory onto the YZ plane is close to the straight line crossing the beam–target intersection area. A typical experimental distribution of the track parameters in the YZ plane is shown in Fig. 4. The area inside the tetragon contains the accepted events.

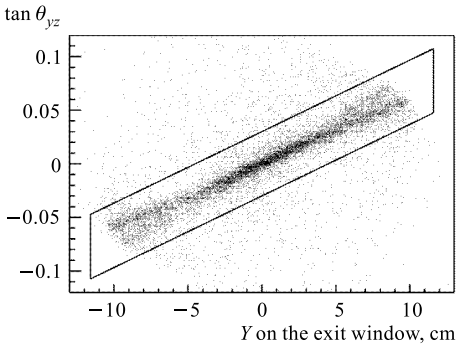

Fig. 4. Correlation of the track parameters in the YZ plane

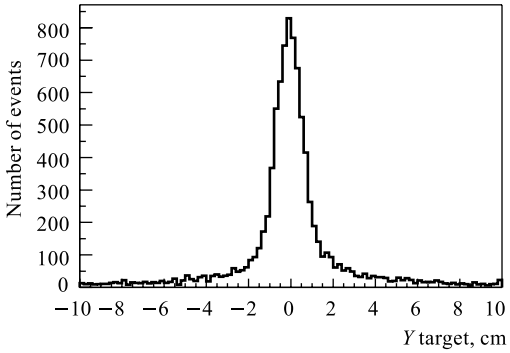

Fig. 5. Reconstructed Y-coordinate of the track in the target region

After application of the criteria mentioned above and reconstruction of the momentum, one can reconstruct the vertical track coordinate in the target region corrected for the magnetic field (Fig. 5). This is done within the same polynomial approximation as the three-momentum reconstruction and allows for application of a finer background rejection criterion.

The background cut parameters are found at a separate calibration step of the data analysis, when all the cuts are released and only events with a single cluster on each wire plane are processed (Figs. 4 and 5 demonstrate an outcome of this step).

3.2. Reconstruction of Single-Track Event. Reconstruction of events with one particle detected can be illustrated with the experimental data obtained with the H_2 target at a proton beam energy of 0.5 GeV.

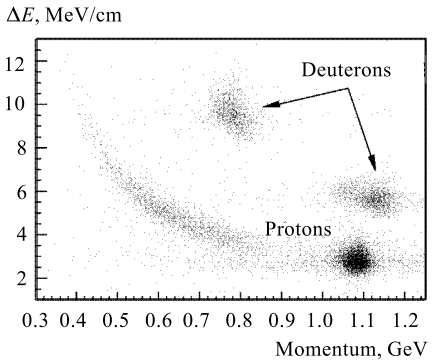

Fig. 6. ΔE versus momentum on the H_2 target at $T_p = 0.5$ GeV

Figure 6 presents an experimental distribution of the energy losses measured in the hodoscope versus the reconstructed particle momentum. One can effectively separate protons and deuterons in the momentum range shown in this figure, where their energy losses are essentially different. At higher momenta a similar separation can be done with the use of the FD Cherenkov counters [2]. In Fig. 7, *a* one can see a distribution of events in the plot of the particle momentum versus the projection of the particle emission angle onto the median plane. (The accepted emission angles in the vertical plane are within $\pm 3.5°$.) The lines show kinematic loci of the reactions $pp \to pp$ and $pp \to d\pi^+$, with the deuteron detected in the latter. The distributions in Fig. 7, *b, c* are obtained after selection of deuterons and protons by energy losses.

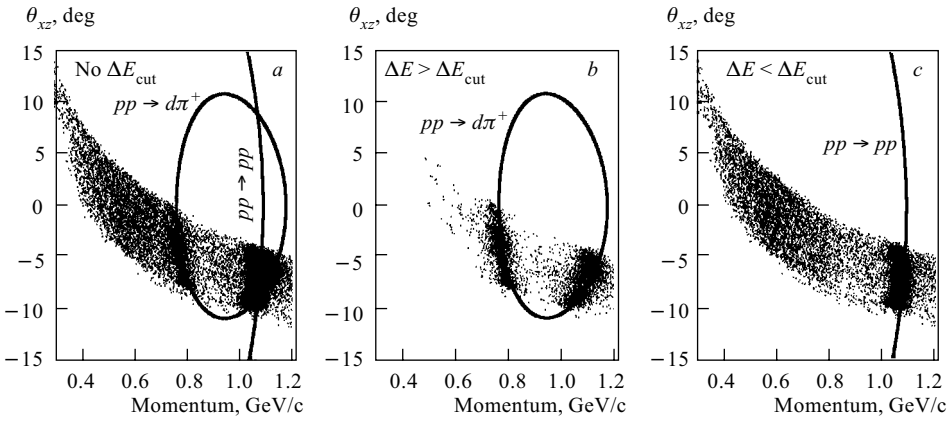

Fig. 7. Acceptance with the H_2 target at $T_p = 0.5$ GeV for: *a*) all events; *b*) deuterons selected by ΔE; *c*) protons selected by ΔE

The *pp* elastic scattering is clearly selectable at all COSY beam energies, which is demonstrated in Fig. 8, where it forms prominent peaks in the momentum spectra. It makes this process suitable for luminosity monitoring in the ANKE experiments.

3.3. Momentum Resolution. Comparison with Simulation. As one can see in Fig. 7, the momentum of elastically scattered protons, accepted in the FD, varies only little with the angle. This allows one to estimate the momentum resolution by selecting protons in

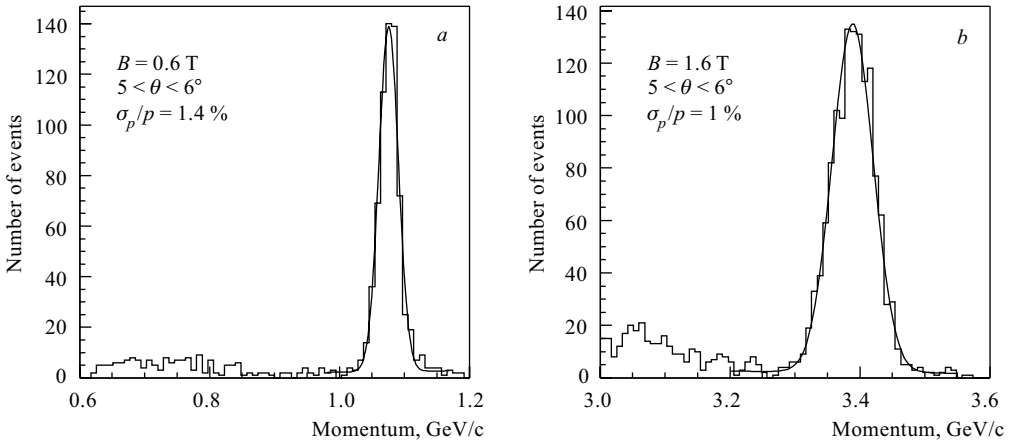

Fig. 8. Momentum spectra of protons at $T_p = 0.5$ (a) and 2.65 GeV (b)

a narrow angular range, as is shown in Fig. 8. In Fig. 9 the curve shows the momentum resolution for protons obtained from a Monte-Carlo simulation at a maximum field of 1.6 T in D2. The uncertainties correspond to ± 1 mm variation of the transversal beam dimension. The experimental resolution is obtained for protons from the elastic pp-scattering reaction measured at two beam energies at the same field value.

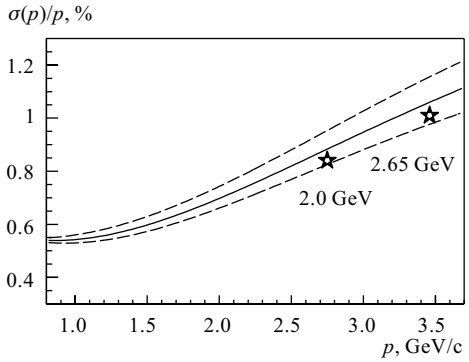

Fig. 9. Momentum resolution for protons. The solid curve is the expected resolution, the dashed curves show its uncertainties. The stars present the experimental resolution of elastically scattered protons at $T_p = 2.0$ and 2.65 GeV

One can also compare the expected and experimental missing mass resolutions in reactions with fully reconstructed kinematics. In our case these are the reactions with two or three particles in the final state, with one or two of them detected, respectively. Such a comparison was done in a number of cases, including the reactions $pp \to d\pi^+$ and the elastic pp scattering, and showed good agreement of the expected and experimental resolutions. For example, in the deuteron breakup $pd \to ppn$ experiment the two final protons have to be detected in the FD, and the main identification criterion of the process employs the value of their missing mass M_x^{pp}. The experimental resolution at $T_p = 0.6$ GeV is $\sigma(M_x^{pp}) = (17.5 \pm 0.7)$ MeV, while the simulation gives a value $\sigma(M_x^{pp}) = 17$ MeV.

3.4. Reconstruction of Double-Track Events. To demonstrate the reconstruction of double-track events, we present data obtained with the H_2 and D_2 targets for a proton beam energy of 0.7 GeV. Particular attention is paid to identification of the $pd \to ppn$ reaction with a small excitation energy in the (pp) pair. (The excitation energy E_{pp} is the total kinetic energy of the pair in its center-of-mass system.)

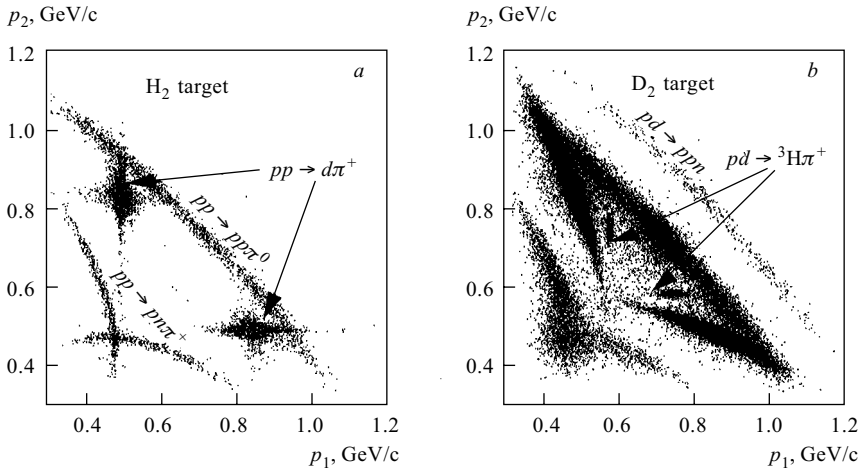

Fig. 10. Momentum correlation in double-track events for the data taken with the H_2 (*a*) and D_2 (*b*) targets at the beam energy $T_p = 0.7$ GeV

3.4.1. Momentum Correlation. The absolute values (P_1 and P_2) of the momenta of two particles in any three-particle final-state process are strictly correlated if the particles are emitted at fixed directions (θ_1, ϕ_1 and θ_2, ϕ_2). The correlation is conserved to some extent if the emission angles slightly vary within small restricted solid angles around the θ_1, ϕ_1 and θ_2, ϕ_2 directions. Rather limited angular acceptance of the FD results in significant correlation between the momenta of two detected particles in any three-particle final-state process. The advantage of such a kinematic correlation is a distinctive clustering of the observed events with different masses of particles in the plot (P_1, P_2). Therefore, separation of the processes can be done without preceding identification of the particle.

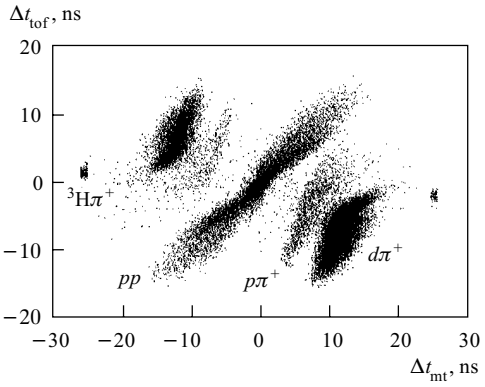

Fig. 11. Time-of-flight difference calculated under the assumption of two protons detected ($\Delta_{\rm tof}$) versus the one measured in the hodoscope ($\Delta_{\rm mt}$). The data are taken with the D_2 target at $T_p = 0.7$ GeV

Figure 10 demonstrates such a correlation. The processes $pp \to pp\pi^0$, $pp \to d\pi^+$ and $pp \to p\pi^+ n$ (Fig. 10, *a*) are well separated, though only the particle momenta were used. With the D_2 target (Fig. 10, *b*), one observes some smoothing of the corresponding groups due to a quasi-free character of the processes at nucleons in the deuteron. In addition, some other processes, possible only with the use of a deuterium target, appear in the plot: $pd \to ppn$, $pd \to {}^3H\pi^+$.

The observed correlation can be used to identify the processes and the masses of particles involved.

3.4.2. Use of Time-of-Arrival Difference. Double-particle events allow the time-of-flight information to be gained even when only the forward detector, without any other detector

group of the spectrometer, is used. Then for events with particles hitting two different hodoscope counters, the time-of-arrival difference $\Delta_{\rm mt}$ is measured as a difference between the time measured in each counter. On the other hand, assuming a definite mass for both particles, one can calculate the time-of-flight difference $\Delta_{\rm tof}$ in accordance with their measured 3-momenta. Then, if the assumption is correct, $\Delta_{\rm tof}$ should be equal to $\Delta_{\rm mt}$. In Fig. 11 a distribution of the pairs in the plot ($\Delta_{\rm mt}$, $\Delta_{\rm tof}$) obtained under the assumption of both particles being protons reveals a clustering of the pp events along the diagonal $\Delta_{\rm tof} = \Delta_{\rm mt}$, while the other pairs occupy different areas of the plot. Choice of the appropriate cuts allows suppression of the background and selection of the desired pairs of particles.

3.4.3. Selection of Proton Pairs with a Small Excitation Energy. Although the range of excitation energy E_{pp} for detected pairs extends up to ≈ 200 MeV, the acceptance for pairs with E_{pp} higher than 3–10 MeV (depending on the beam energy) becomes very low. Nevertheless, the setup acceptance for pairs with E_{pp} below 3 MeV remains rather high in the beam energy range 0.5–2.0 GeV. This allows the study of reactions with production of a fast proton pair with a low excitation energy in the pair. The favorable circumstance is a decrease in the measurement error $\sigma(E_{pp})$ with decreasing of the energy. Figure 12 shows the simulated energy dependence of $\sigma(E_{pp})$. It is seen that, for $E_{pp} < 3$ MeV, $\sigma(E_{pp})$ becomes less than 0.3 MeV, which makes it possible to study the final-state interaction in the processes with two protons in the final state. Figure 13 shows the event distribution over the excitation

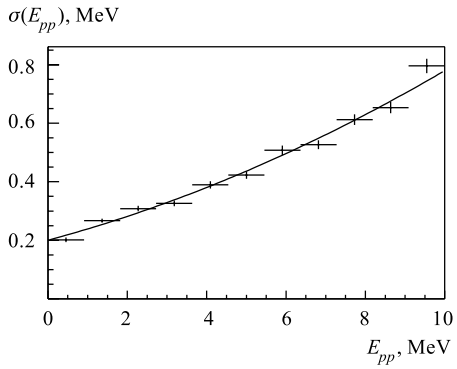

Fig. 12. Simulated resolution in the (pp) excitation energy in the reaction $pd \to ppn$ at $T_p = 0.7$ GeV. The line is a polynomial fit of the points

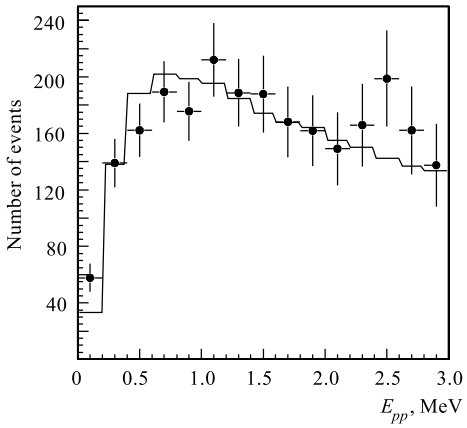

Fig. 13. Distribution over the excitation energy E_{pp} in comparison with the theoretical expectation (histogramm) from final-state interaction

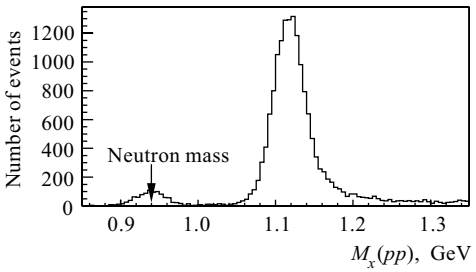

Fig. 14. Missing mass spectrum in the $pd \to ppX$ process at $T_p = 0.7$ GeV

energy E_{pp} in the process $pd \to ppn$ for the T_p energies 0.6–0.8 GeV. The shape of the spectrum is well reproduced ($\chi^2/\mathrm{n.d.f.} = 0.99$) by the phase space distribution multiplied by the Migdal–Watson final-state interaction factor with Coulomb interaction [11].

3.4.4. Example of Process Identification in the FD. A missing mass spectrum of the process $pd \to ppX$ at a beam energy of 0.7 GeV is shown in Fig. 14. The proton pairs are selected by the time-of-arrival difference. The spectrum reveals a clear peak at a value close to the neutron mass. This means that events from this peak belong to a rare process of the proton-induced deuteron breakup with forward emission of a proton pair. The differential cross section of the process is found in [12]. At a beam energy of 1.9 GeV the cross section decreases to the level of 30 nb/sr.

CONCLUSION

The forward detector system of the ANKE spectrometer makes it possible to study a wide range of intermediate-energy processes at rather low cross sections and with an acceptable accuracy. It is used in the majority of the experiments being performed at ANKE: deuteron breakup at high-momentum transfer [12], correlation experiments on subthreshold K^+ production [13], ω-meson production in pd collisions [14], a^0-meson production [15], and others.

Acknowledgments. We are grateful to the COSY accelerator staff for providing proper conditions for tuning and performance study of the setup. We also thank the IKP FZJ and LNP JINR management for the permanent support of this work. This work was supported by the BMBF WTZ grants RUS 00/211 and RUS 01/619.

REFERENCES

1. *Barsov S. et al.* ANKE, a New Facility for Medium Energy Hadron Physics at COSY–Jülich // Nucl. Instr. Meth. A. 2001. V. 462. P. 364.

2. *Chiladze B. et al.* The Forward Detector of the ANKE Spectrometer. Scintillation and Cherenkov Hodoscopes // Part. Nucl., Lett. 2002. No. 4[113].

3. *Zalikhanov B. Zh. et al.* Development of the Forward Detector for the 0°-Facility. IKP FZ-Jülich Annual Report 1993, IKP Jül-2879. Jülich, 1994. P. 57.

4. *Zalikhanov B. Zh. et al.* First Module of the Forward Proportional Chamber of the ANKE Spectrometer. IKP FZ-Jülich Annual Report 1995, IKP Jül-3200. Jülich, 1996. P. 67.

5. *Petrus A. Yu., Zalikhanov B. Zh.* Electro-Mechanical Properties of Narrow-Gap Multiwire Proportional Chambers // Nucl. Instr. Meth. A. 2002. V. 485. P. 399.

6. *Kalmar H. et al.* // Nucl. Instr. Meth. A. 1991. V. 307. P. 279.

7. *Petrus A. Yu.* Multiwire Proportional Chamber with a Dielectric Film. Numerical Study. JINR Commun. E13-2002-14. Dubna, 2002.

8. *Borchert G. et al.* An Economic Wire Chamber Readout and Data Acquisition System for ANKE. IKP FZ-Jülich Annual Report 1997, IKP Jül-3505. Jülich, 1998. P. 59.

9. GEANT – Detector Description and Simulation Tool. CERN Program Library Long Writeup W5013.

10. *Volkov A. D. et al.* Method for the Calculation of Charged Particle Momentum in Magnetic Spectrometers // Nucl. Instr. Meth. A. 1991. V. 306. P. 278.

11. *Watson K. M.* // Phys. Rev. 1952. V. 88. P. 1163;
Migdal A. B. // Sov. Phys. JETP. 1955. V. 1. P. 2.

12. *Komarov V. et al.* Proton-Induced Deuteron Breakup at GeV Energies with Forward Emission of a Fast Proton Pair // Phys. Lett. B. 2003. V. 553. P. 179.

13. *Koptev V. et al.* Observation of K^+d Correlations from pA Collisions. Submitted for publication in «Eur. Phys. J. A» (2003).

14. *Barsov S. et al.* Near-Threshold Production of Omega Mesons in the $pn \to d\omega$ Reaction. To be submitted to «Phys. Lett. B».

15. *Kleber V. et al.* $a_0^+(980)$-Resonance Production in $pp \to dK^+\overline{K}^0$ Reactions Close to Threshold. Submitted for publication in «Phys. Rev. Lett.» (2003).

Received on September 4, 2003.